Fabrication of porous Ag hollow sphere arrays based on coated template-plasma bombardment

2013 Nanotechnology 24 465302

(http://iopscience.iop.org/0957-4484/24/46/465302)

Nanotechnology **24** (2013) 465302 (8pp) doi:10.1088/0957-4484/24/46/465302

Fabrication of porous Ag hollow sphere arrays based on coated template-plasma bombardment

Hui He[1], Weiping Cai[1], Zhengfei Dai[1], Guangqiang Liu[1] and Hanhe Li[2]

[1] Key Laboratory of Materials Physics, Anhui Key Laboratory of Nanomaterials and Nanotechnology, Institute of Solid State Physics, Chinese Academy of Sciences, Hefei 230031, People's Republic of China
[2] Agricultural Machinery Appraisal Station, Hubei University of Technology, Wuhan 430068, People's Republic of China

E-mail: wpcai@issp.ac.cn

Received 1 August 2013, in final form 11 September 2013
Published 22 October 2013
Online at stacks.iop.org/Nano/24/465302

Abstract

A facile and flexible strategy is presented to produce porous Ag hollow sphere arrays, with a micro/nanostructure and contaminant-free surface, based on a combination of the bottom-up and top-down fabrication strategies, or by plasma bombardment of Ag-coated monolayer polystyrene sphere templates. The arrays consist of periodically arranged micro-sized hollow spheres with nanoscaled pores (mostly within 100 nm) in the shell layer. These arrays are structurally tunable in spherical size (in the sub-10 μm range), spacing (from a few nanometers to several microns), shell thickness (over tens of nanometers) and porous configuration by the template and bombarding conditions. The strategy is universal for the fabrication of other porous metal hollow sphere arrays. Such nanoscaled rough and porous Ag hollow sphere arrays have potential applications in catalysis, antibacterial and photonic devices. The arrays show significant surface-enhanced Raman scattering (SERS) activity (the minimum detectable concentration of the standard molecule rhodamine 6G can be down to 10^{-14} M) with good stability and reproduction, and are a good candidate for the substrate of SERS effect based devices.

S Online supplementary data available from stacks.iop.org/Nano/24/465302/mmedia

(Some figures may appear in colour only in the online journal)

1. Introduction

Ag hollow spheres and their arrays have received considerable attention recently owing to their unique properties and potential applications in catalysis [1, 2], antibacterial activity [3, 4], and solar cells [5, 6], etc. In particular, they are excellent substrates for surface-enhanced Raman scattering (SERS) sensors due to their tunable surface plasmon resonance over a broad range and large surface area to adsorb the detected molecules [7–10]. Several fabrication techniques have been developed, including microemulsion [11], chemical reduction [12], electroless plating [13], hydrothermal assembly [14], thermal decomposition [15], spray pyrolysis [16], template routes (amphiphilic graft copolymers [17], polyelectrolyte capsule [18], nanoparticles [19], SiO_2 nanospheres [20, 21], and polymer colloidal spheres [22, 23]), etc. All these techniques are based on the bottom-up nanofabrication strategy. Generally, it is difficult to obtain a Ag hollow sphere combining the advantages of both roughness and porosity for better performances. Furthermore, to our knowledge, there are few reports [24] on fabrication of patterned Ag hollow spheres with tunable structures which are vitally important for practical applications.

Our motivation is to construct the novel Ag hollow sphere arrays (HSAs) with features including high roughness and dense nanopores based on a combination of the bottom-up and top-down fabrication strategies. We present a flexible and simple way to fabricate porous Ag HSAs with controllable and tunable structures based on the strategy of plasma bombardment on a Ag-coated polystyrene (PS) colloidal monolayer template, as illustrated in scheme 1. First, the non-close-packed PS colloidal monolayer was coated with Ag by ion beam sputtering deposition and subsequently removed by dissolution. The Ag HSA was thus left. Then, plasma

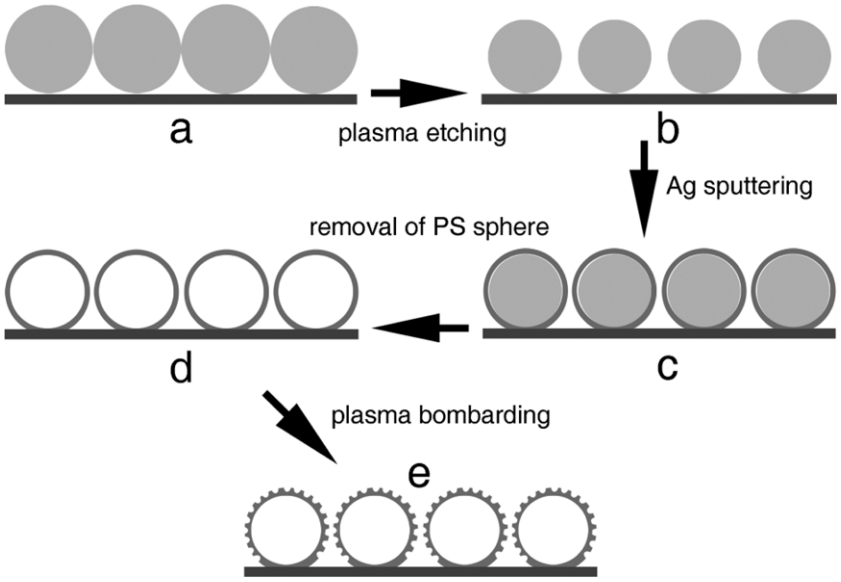

Scheme 1. Schematic illustration for the fabrication of porous Ag hollow sphere array based on the combination of bottom-up and top-down strategies. (a) a close packed PS sphere monolayer template on a silicon substrate. (b) Ar plasma etching-induced non-close packed PS sphere monolayer on the silicon substrate. (c) Ag-coated non-close packed PS sphere monolayer by ion-sputtering deposition. (d) Ag hollow sphere array after removal of the inner PS spheres. (e) porous Ag hollow sphere array after Ar plasma bombardment.

bombardment was performed on the Ag HSA, and a porous Ag HSA with a clean surface was finally obtained. The array is contaminant-free, built of hollow spheres with porous Ag shell layers, and homogeneous in macro-size. The spherical shell-blocks are micro/nanostructured with evenly distributed nanopores which cannot penetrate through the shell surface. This array is structurally tunable in spherical size, spacing, shell thickness and porous configuration by the template and bombardment conditions. Such a hierarchically porous HSA is very useful in catalysis, sensors, and nanodevices. It exhibits significantly structurally enhanced SERS activity with good stability and reproduction due to its unique structure. This strategy is generally applicable for the fabrication of other hierarchically porous metal HSAs.

2. Experimental section

2.1. Preparation of PS templates on Si-wafer

A PS suspension (containing 2.5 wt% colloidal spheres 1 μm in diameter, surfactant-free) was purchased from Alfa Aesar Corporation. The uniform PS colloidal monolayer with several square centimeters in dimension was prepared on a well cleaned glass slide by a gas–liquid–solid interface self-assembly method, as previously reported [25]. In brief, the PS suspension and ethanol at a volume ratio of 1:1 were mixed. The ordinary glass slide (7.5 $\times$ 2.5 cm^2) was cleaned in turn with acetone, ethanol, 98% H_2SO_4/H_2O_2 (3:1 in volume), $H_2O/NH_3 \cdot H_2O/H_2O_2$ (5:1:1 in volume), and deionized water. After the glass slide was dried, an appropriate amount of deionized water was dropped above it to form a water film. About 150 ml of the mixed suspension was pipetted onto the water film at its boundary location. Then, a large area colloidal monolayer was formed after liquid evaporation by using a gentle airflow at 30 °C. The monolayer was then picked up with a cleaned silicon wafer, followed by heating at 110 °C for 10 min, for a good contact between PS spheres and Si substrate. We thus obtained a close-packed PS colloidal monolayer on a Si-wafer. Plasma etching of the PS colloidal monolayer was performed to form a non-close-packed monolayer template, using an argon plasma cleaner (PDC-32G-2) with 18 W power for 6 min, as previously reported [26, 27]. The spacing between adjacent etched PS spheres was tuned by etching time. Longer etching time led to a larger sphere spacing and a smaller sphere size.

2.2. Ag coating

Silver was subsequently deposited or coated on the etched PS colloidal template on the Si-wafer by using a commercial ion beam sputtering system at a pressure of 7.5 $\times$ 10^{-5} Torr (Shenyang City Keyou Institute of Vacuum Technology, China) [28]. Ar was used as shielding gas. Acceleration voltage was 1.2 kV, and ion current was 2.5 mA. The deposition rate was about 0.1 nm s^{-1}, and the coating thickness was controlled by sputtering time. After deposition, the inner PS spheres were removed by dissolution in CH_2Cl_2 solution with ultrasonic vibration. An hexagonally arranged Ag hollow sphere array was thus obtained. For reference, a continuous Ag thin film was also prepared on the Si substrate without the PS spheres under the same sputtering conditions.

2.3. Plasma bombardment and characterization

The Ag HSAs and the corresponding continuous thin film were bombarded using radio-frequency (RF)-excited Ar plasma, in an argon plasma cleaner (PDC-32G-2, Harrick

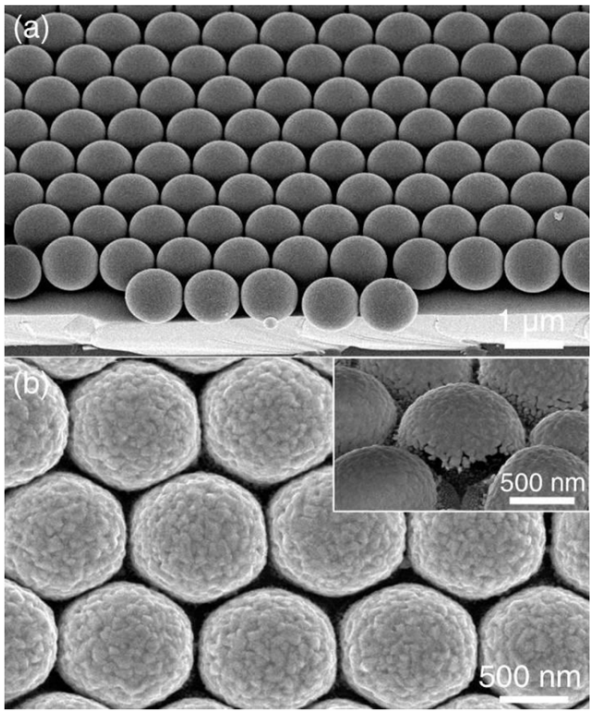

Figure 1. FESEM images of the etched PS colloidal monolayer before (a), and after Ag coating (about 70 nm in thickness) and subsequent removal of the PS spheres (b). Inset in (b): the image with a broken sphere in the edge region of the sample.

Plasma Co.) at a pressure of 0.15 Torr and an input power of 18 W for 40 min. The flow rate of Ar gas was 8 SCFH (standard cubic feet per hour).

The samples were examined by field-emission scanning electron microscope (FESEM, Sirion 200). X-ray diffraction (XRD) measurements were conducted on a Philips X'Pert instrument with Cu Kα radiation. Optical absorption spectra were recorded on a spectrophotometer (Cary 5E UV/vis–NIR). For SERS spectral examination, the samples (0.5 cm $\times$ 0.5 cm) were immersed in 10 ml of rhodamine 6G (R6G) aqueous solutions with different concentrations for 10 min, then taken out and immediately dried with high-purity flowing nitrogen. Raman spectral measurements were conducted on a French LABRAM-HR confocal laser microRaman spectrometer with a laser wavelength of 785 nm and a laser beam spot of 10 μm on the sample. Laser power was 10 mW.

3. Results and discussion

Figure 1(a) shows a typical morphology of the etched PS colloidal monolayer, which is hexagonally arranged. After ion beam sputtering, the PS spheres were coated with Ag layer. The coating shells surrounding the PS spheres are not dense but porous. So the subsequent immersion into the CH_2Cl_2 solution with ultrasonic vibration would lead to dissolution or removal of the PS spheres. We can thus obtain a homogeneous monolayer hollow sphere array with a centimeter squared dimension. Figure 1(b) illustrates the typical result, corresponding to the sample after Ag sputtering

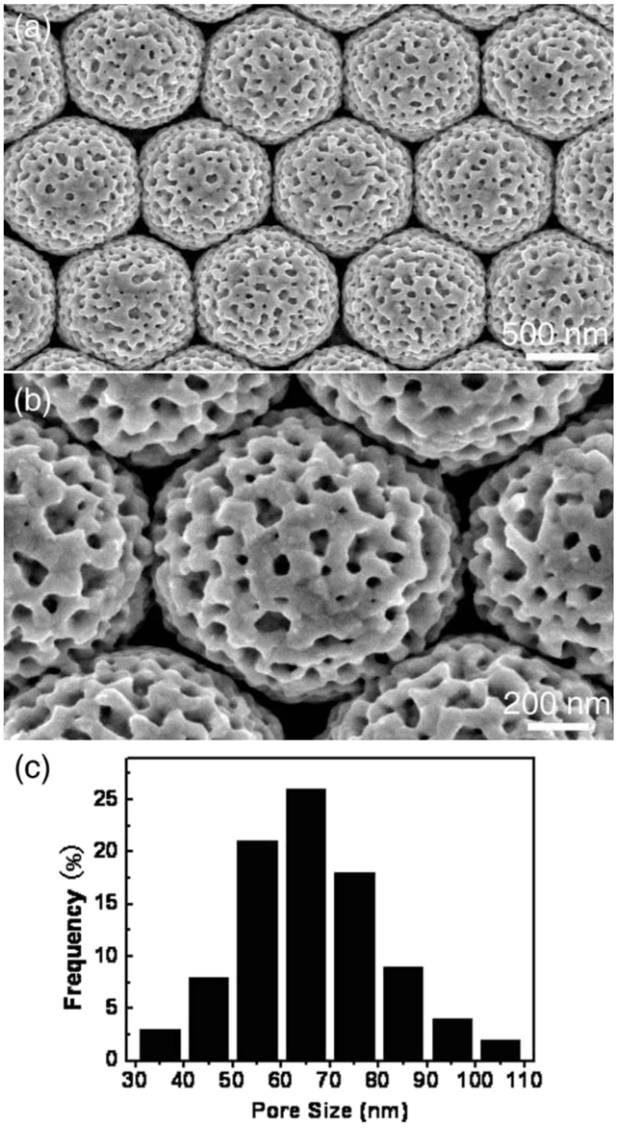

Figure 2. FESEM images of the sample, shown in figure 1(b), after plasma bombardment for 40 min with power of 18 W ((a), (b)), and pore size distribution (c).

for 12 min (about 70 nm in the coating thickness) and removal of PS spheres, showing the hollow structure (see the image with a broken sphere, inset in figure 1(b)). The formation of such spherical shells is attributed to the ion-sputtering-induced nonshadow deposition [29, 30]. XRD revealed that the obtained film is Ag with fcc structure (figure S1 available at stacks.iop.org/Nano/24/465302/mmedia). The Ag hollow spheres are composed of nanoparticles tens of nanometers in size and are still well isolated from each other. It should be pointed out that the shell thickness near the top part of the spheres is slightly bigger than that at the lower part due to the different accessibility of the sputtered Ag atoms/clusters to different places.

3.1. Morphologies and structure

After Ar plasma bombardment on the Ag HSA for 40 min, numerous nanopores are formed uniformly on the spherical shell surface over the whole sample, as shown in figure 2(a)

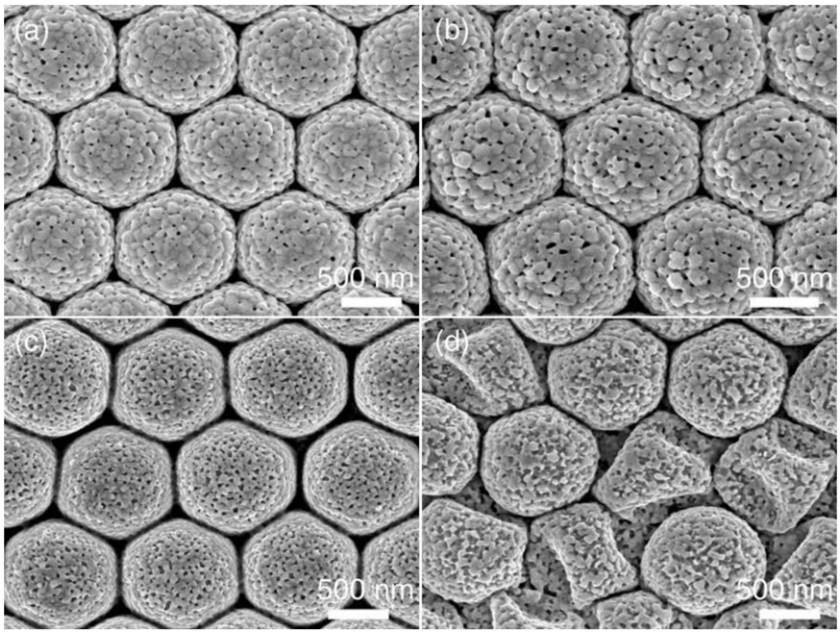

Figure 3. Morphological evolution with plasma bombarding time for the Ag HSA shown in figure 1(b) (power: 18 W). (a) 5 min. (b) 10 min. (c) 20 min. (d) 60 min.

due to isotropic plasma bombardment on the Ag hollow spheres. All the hollow spheres remain of spherical profile without distortion and exhibit an open-cell spongelike morphology. Careful examination of the high-magnification SEM image (figure 2(b)) reveals that these nanosized pores are non-through and irregular, and of nanometers to tens of nanometers in scale (figure 2(c)). Compared with the original state (figure 1(b)), the Ag nanoparticles have changed in shape and the particles' boundaries have become undistinguishable. As a whole, such porous Ag hollow spheres are micro/nanostructured, and the constructed periodic array is homogeneous in the macroscale but hierarchically rough and porous in the nanoscale. In addition, the array should be contaminant-free on the surface due to the plasma bombardment during preparation. EDX analysis has been done for such porous array (figure S2 available at stacks.iop.org/Nano/24/465302/mmedia). There are only the Ag peak, and the Si peak from the Si substrate, demonstrating a clean surface. Hence, plasma bombardment is an effective technique for surface micromachining of Ag films.

3.2. Influential factors

Further experiments have revealed that plasma power, plasma bombarding time and Ag coating thickness are the key influential factors for formation of the homogeneous porous shell.

3.2.1. Bombarding time and power. Figure 3 shows the morphological evolution with bombardment at the power 18 W for the Ag HSA shown in figure 1(b). When bombardment is for a short time (say, 5 min), only a few shallow nanopits are observed on the shell surface (figure 3(a)). With increasing time, the nanopits increase in number and size (figures 3(b) and (c)). When the bombarding duration is long enough (say, 40 min in this study), the homogeneous porous structure can be obtained in the shell layer (figure 2). However, too long a plasma bombardment leads to distortion or damage of the Ag hollow spheres, as shown in figure 3(d).

Similarly, plasma power also has an important influence on the number and size of nanopores. If we use low bombarding powers, only some small nanopores are observed and increasing power induces the more and bigger nanopores, as shown in figure 4 corresponding to the sample shown in figure 1(b) after bombardment for 40 min with the powers 6.8 and 10.5 W. In contrast, too high a power will lead to damage of the hollow spherical structure. Only the appropriate power can induce the homogeneous porous spherical shell. In our case, a power of about 18 W is enough to obtain a perfect result, as illustrated in figure 2.

3.2.2. Thickness of the coated layer. The modified morphology of the shell depends strongly on Ag coating thickness which is controlled by sputtering time. Figure 5 shows the results corresponding to the Ag shells with different thicknesses after plasma bombardment for 40 min with the power of 18 W. If the Ag coating was too thin (say, $<$50 nm), the hollow spheres could collapse after plasma bombardment because the thin shells are not strong enough (figures 5(a) and (b)). Contrarily, when the Ag coating was too thick (say, $>$90 nm), the nanopores in the shells decrease in number and distribute inhomogeneously (figures 5(c) and (d)). Only with suitable shell thickness (within tens of nanometers) can numerous nanopores with even distribution be obtained, as shown in figure 2.

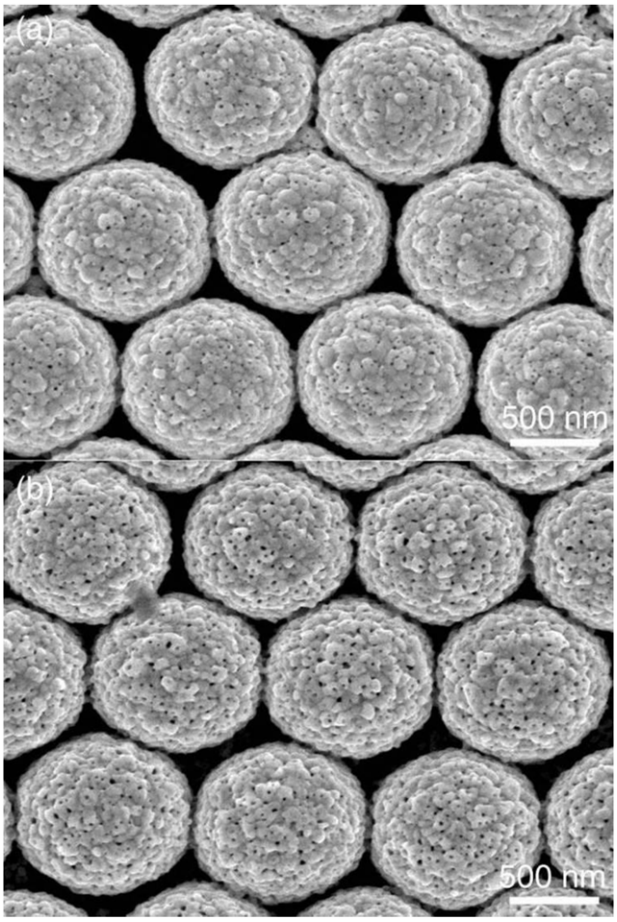

Figure 4. Influence of the bombarding power on the morphologies of the sample shown in figure 1(b) (bombarding time: 40 min). (a) 6.8 W. (b) 10.5 W.

3.3. Formation of homogeneous nanopores

The plasma bombardment-induced formation of nanopores on the spherical shell surface is easily understood. Ag, unlike other metals, has a high surface mobility, even at room temperature [31]. During isotropic plasma treatment, the Ar^+ ion bombardment will induce densification and even surface melting (and/or slight sputtering) of the deposited Ag coating, due to energy transferring. For the samples with thick enough coating, such densification will result in contraction of the Ag shells and hence formation of nanoholes or nanopits on the cupped sites, as shown in figure 2. Also, surface melting leads to a smooth surface (see figures 2(b) and 5(c)). For the samples with thin coating, which is of lower heat capacity, the spherical morphology will be destroyed due to a melting-induced weakening (see figures 5(a) and (b)). For the deposited 2D Ag film on planar Si-wafer, heat on the Ag surface should be easily transferred to the substrate due to the planar contact and the Ag melting degree is thus decreased, which results in the nanopores on such film being smaller than those on the spherical shells under the same experimental conditions, as demonstrated in figure S3 (available at stacks.iop.org/Nano/24/465302/mmedia) and figure 2. Additionally, compared with those before plasma bombardment, the average thicknesses on top and bottom of the Ag spherical shells and the Ag film are almost unchanged, as a result of slight Ag sputtering.

It should be pointed out that plasma bombardment is a different process from annealing which can heat the entire Ag hollow spheres and induce their thermal deformation. Figure S4 (available at stacks.iop.org/Nano/24/465302/mmedia) gives the morphologies corresponding to the Ag HSA shown in figure 1(b) after annealing

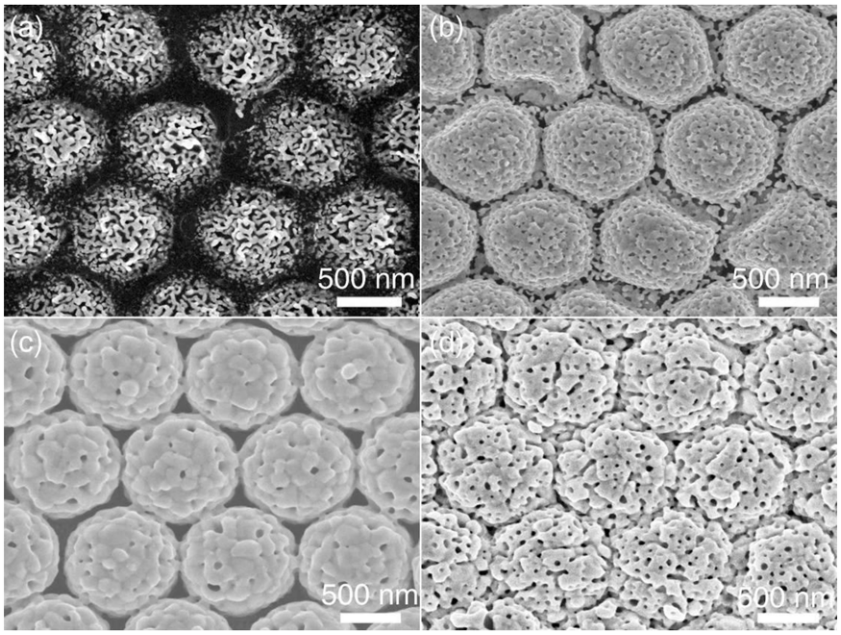

Figure 5. Influence of Ag coating thickness on the morphologies of the porous HSAs (power: 18 W, bombarding time: 40 min). (a) 20 nm. (b) 50 nm. (c) 90 nm. (d) 140 nm.

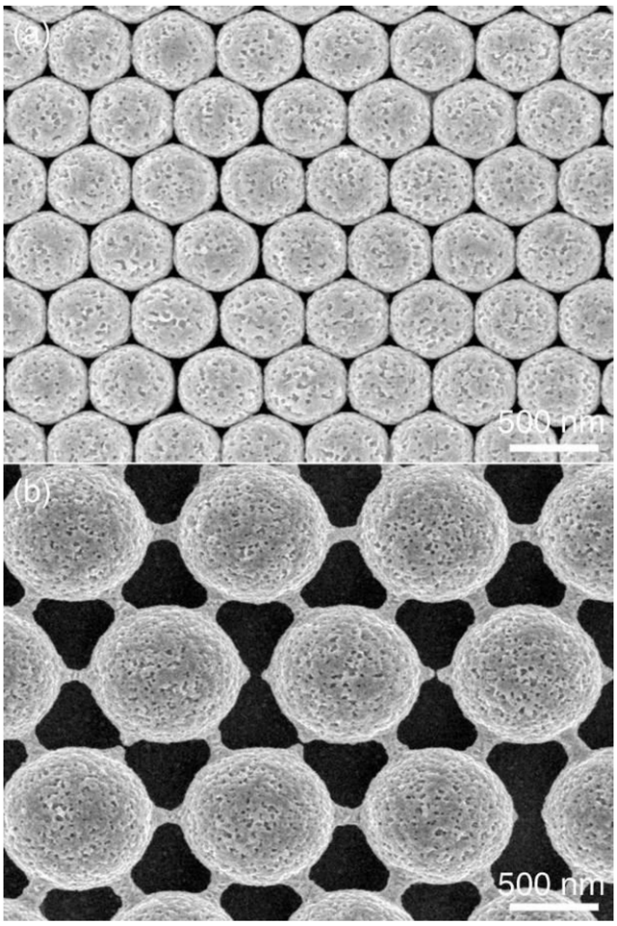

Figure 6. Morphologies of the porous Ag HSAs from other PS templates (70 nm in Ag coating thickness, plasma bombardment for 15 min with power of 18 W). (a) 500 nm PS monolayer. (b) 1000 nm PS monolayer after plasma etching for a longer duration (the neck connection can be removed by subsequently heating the etched PS spheres).

for 20 min at different temperatures. After annealing at 300 °C, all the Ag hollow spheres collapse with some nanopores, which originates from heating-induced contraction (figure S4(a) available at stacks.iop.org/Nano/24/465302/mmedia); annealing at 400 °C induces big Ag particles (figure S4(b) available at stacks.iop.org/Nano/24/465302/mmedia). Therefore, plasma bombardment is a good technique for surface morphological modification.

3.4. Extension of the strategy

The structural parameters of the porous Ag HSA are tunable by PS sphere template configuration. Figure 6 shows the morphologies of the porous HSAs with smaller spheres and larger spacings. The easy control of size (in the sub-10 μm range) and spacing (from a few nanometers to several microns) for such an array is important for functional optimization or structure-related quantitative study of physical properties. In addition, the strategy presented in this study can be extended to fabricate other porous metal HSAs. For instance, a porous Au HSA can be obtained (figure S5 available at stacks.iop.org/Nano/24/465302/mmedia) by similar process.

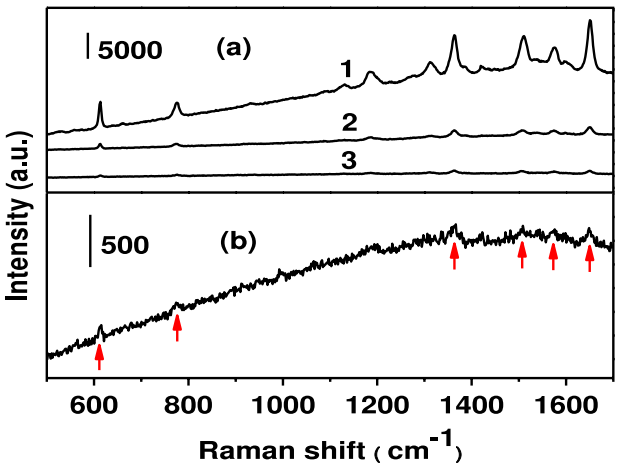

Figure 7. Raman spectra of R6G molecules on different substrates. (a) 10^{-9} M R6G, the integration time = 5 s. Curve 1: the porous Ag HSA shown in figure 2. Curve 2: the sample shown in figure 1(b) (without plasma bombardment). Curve 3: the Ag continuous thin film (without using PS spheres, shown in figure S3 available at stacks.iop.org/Nano/24/465302/mmedia). (b) 10^{-14} M R6G, the integration time = 15 s. Curve in (b): the porous Ag HSA shown in figure 2. (The arrows in (b) show some characteristic peaks.)

3.5. SERS properties

The hierarchically porous HSA, as mentioned above, is very useful in catalysis, sensors, and nanodevices. Here, we take the SERS performance of the sample shown in figure 2 as an example to demonstrate its usability as a SERS-based device. It exhibits significant SERS activity with good stability and reproduction due to its unique structure.

3.5.1. Enhanced SERS activity. Using R6G as the probe molecules, the hierarchically porous Ag HSA shown in figure 2 exhibited a significantly structurally enhanced SERS activity under normal Raman excitation wavelength of 785 nm (chosen according to its optical absorption spectra shown in figure S6 available at stacks.iop.org/Nano/24/465302/mmedia), as shown in figure 7(a). It can be seen that the SERS activity of the porous HSA is much higher than that of the original one without plasma bombardment and the plasma-bombarded continuous thin film (figure S3 available at stacks.iop.org/Nano/24/465302/mmedia). Further, for the porous Ag HSA, the minimum detectable concentration of R6G can be down to 10^{-14} M when using a short integration time (15 s) (figure 7(b)), which shows the possibility of molecule-level detection. Correspondingly, for the original Ag HSA without plasma bombardment and for the plasma-bombarded continuous film, there are no detectable signals.

Compared with the HSA without plasma bombardment, we know that the nanopores on the Ag shell layer play a dominant role in enhancement of the SERS activity. The strong SERS effect for the hierarchically porous Ag HSA

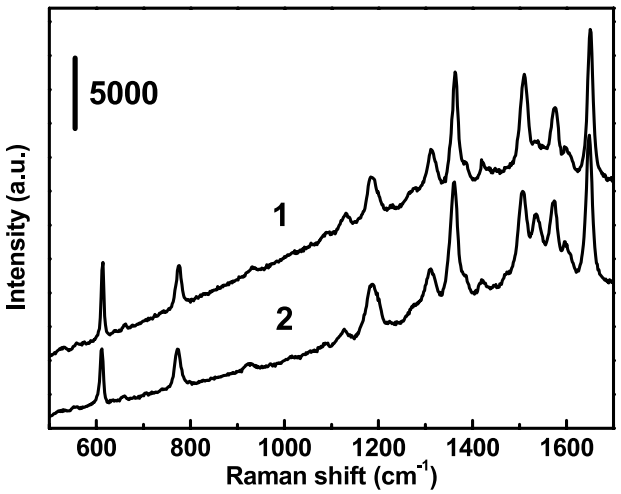

Figure 8. Raman spectra of 10^{-9} M R6G on the porous Ag HSA shown in figure 2 without (curve 1) and with (curve 2) the experience of immersion in water for two weeks. Data integration time = 5 s.

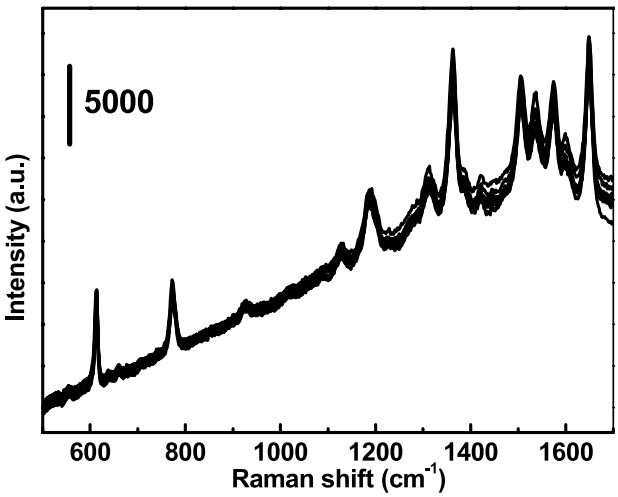

Figure 9. Raman spectra of 10^{-9} M R6G collected from 9 randomly selected sites on the porous Ag HSA shown in figure 2. Data integration time = 5 s.

should be attributed to its unique structure, including the efficient coupling among the nanoscaled interstitials on and between the micro-sized Ag hollow spheres, the greater surface area exposed to the environment, and the increased density of optical modes induced by the periodic structure [32, 33]. Upon optical excitation, these hot spots, especially the hottest ones, support extremely intense local electromagnetic fields and thus induce strong Raman signal of the local adsorbed probe molecules [34–36]. The hierarchically porous Ag HSA in this study has two advantages. Firstly, plasma bombardment can remove organic contamination (PS and/or CH_2Cl_2, if any), which is advantageous for adsorption of the detected molecules. Secondly, the array structure can easily lead to a nice signal uniformity, and is tunable, by multi-structural parameters, for further optimization of SERS activity.

3.5.2. Stability and reproducibility. A desirable SERS substrate should be stable and durable in an aqueous solution [37, 38]. Figure 8 gives the results of the SERS activity for the porous Ag HSA shown in figure 2 before and after immersion in deionized water for 2 weeks. Evidently, neither a shift in the major Raman peaks nor a significant change in Raman intensity occurs for the substrate soaked in water for 2 weeks, revealing that it is stable for at least a 2-week period. This long-term stability in water is of great importance for SERS-based devices in practical applications.

It is well known that the poor reproducibility of Raman signals in traditional SERS analysis has been a main obstacle to the use of SERS as a routine analytical tool [39–41]. We collected SERS spectra of R6G from 9 randomly selected positions on the porous Ag HSA shown in figure 2, as shown in figure 9, exhibiting very good measurement reproducibility across the whole substrate (<10% in standard deviation for the main peaks). This is attributed to the highly homogeneous structure of such array.

4. Conclusions

In summary, a facile and flexible strategy is presented to fabricate hierarchically porous Ag hollow sphere arrays based on plasma bombardment of Ag-coated PS colloidal monolayers. The arrays are composed of periodically arranged micro-sized hollow spheres with nanoscaled porous structure in the shell layer, due to isotropic Ar^+ bombardment. The array architecture can be easily tuned by the PS template. Only under special conditions, of suitable plasma power, enough bombardment time, and certain coating thickness, can the homogeneous porous configuration be obtained. Importantly, such nanoscaled rough and porous Ag HSA has potential applications in catalysis, antibacterial and photonic devices. Due to the special structure, it has demonstrated significantly structurally enhanced SERS activity with good stability and reproduction, showing it to be an excellent candidate for the substrate of SERS-based devices. The strategy is universal for the fabrication of other porous metal hollow sphere arrays.

Acknowledgment

This work is financially supported by the Natural Science Foundation of China (Grant Nos 11374303 and 51101149).

References

[1] Liu H, Qu J L, Chen Y F, Li J Q, Ye F, Lee J Y and Yang J 2012 Hollow and cage-bell structured nanomaterials of noble metals *J. Am. Chem. Soc.* **134** 11602–10
[2] Christopher P, Xin H L and Linic S 2011 Visible-light-enhanced catalytic oxidation reactions on plasmonic silver nanostructures *Nature Chem.* **3** 467–72
[3] Deng Z W, Zhu H B, Peng B, Chen H, Sun Y F, Gang X D, Jin P J and Wang J L 2012 Synthesis of PS/Ag nanocomposite spheres with catalytic and antibacterial activities *ACS Appl. Mater. Interfaces* **4** 5625–32
[4] Homan K A, Chen J, Schiano A, Mohamed M, Willets K A, Murugesan S, Stevenson K J and Emelianov S 2011

Silver–polymer composite stars: synthesis and applications *Adv. Funct. Mater.* **21** 1673–80
[5] Sharifi N, Dadgostar S, Taghavinia N and Irajizad A 2013 Freestanding light scattering hollow silver spheres prepared by a facile sacrificial templating method and their application in dye-sensitized solar cells *J. Power Sources* **225** 46–50
[6] de Arquer F P G, Mihi A, Kufer D and Konstantatos G 2013 Photoelectric energy conversion of plasmon-generated hot carriers in metal–insulator–semiconductor structures *ACS Nano* **7** 3581–8
[7] Oldenburg S J, Westcott S L, Averitt R D and Halas N J 1999 Surface enhanced Raman scattering in the near infrared using metal nanoshell substrates *J. Chem. Phys.* **111** 4729–35
[8] Stiles P L, Dieringer J A, Shah N C and Van Duyne R P 2008 Surface-enhanced Raman spectroscopy *Annu. Rev. Anal. Chem.* **1** 601–26
[9] Liu G Q, Cai W P, Kong L C, Duan G T, Li Y, Wang J J, Zuo G M and Cheng Z X 2012 Standing Ag nanoplate-built hollow microsphere arrays: controllable structural parameters and strong SERS performances *J. Mater. Chem.* **22** 3177–84
[10] Stetciura I Y, Markin A V, Ponomarev A P, Yakimansky A V, Demina T S, Grandfils C, Volodkin D V and Gorin D A 2013 New surface-enhanced Raman scattering platforms: composite calcium carbonate microspheres coated with astralen and silver nanoparticles *Langmuir* **29** 4140–7
[11] Kind C, Popescu R, Müller E, Gerthsen D and Feldmann C 2010 Microemulsion-based synthesis of nanoscaled silver hollow spheres and direct comparison with massive particles of similar size *Nanoscale* **2** 2223–9
[12] Ben Moshe A and Markovich G 2011 Synthesis of single crystal hollow silver nanoparticles in a fast reaction–diffusion process *Chem. Mater.* **23** 1239–45
[13] Liu J B, Dong W, Zhan P, Wang S Z, Zhang J H and Wang Z L 2005 Synthesis of bimetallic nanoshells by an improved electroless plating method *Langmuir* **21** 1683–6
[14] Wang G H, Sun Q, Zhang R, Li W C, Zhang X Q and Lu A H 2011 Weak acid–base interaction induced assembly for the synthesis of diverse hollow nanospheres *Chem. Mater.* **23** 4537–42
[15] Yi R, Shi R R, Gao G H, Zhang N, Cui X M, He Y H and Liu X H 2009 Hollow metallic microspheres: fabrication and characterization *J. Phys. Chem.* C **113** 1222–6
[16] Zheng R B, Guo X L and Fu H 2011 One-step, template-free route to silver porous hollow spheres and their optical property *Appl. Surf. Sci.* **257** 2367–70
[17] Gao K J, Yi J J, Mao J, Li G T and Xu B Q 2013 A general template for synthesis of hollow microsphere with well-defined structure *J. Appl. Polym. Sci.* **128** 1687–96
[18] Yang Z H, Yang L L, Zhang Z F, Wu N Z, Xie J L and Cao W X 2008 Hollow spheres of silver synthesized using polyelectrolyte capsules as microreactors *Colloids Surf.* A **312** 113–7
[19] Chen M H and Gao L 2006 Synthesis and characterization of Ag nanoshells by a facile sacrificial template route through *in situ* replacement reaction *Inorg. Chem.* **45** 5145–9
[20] Lu L H, Capek R, Kornowski A, Gaponik N and Eychmuller A 2005 Selective fabrication of ordered bimetallic nanostructures with hierarchical porosity *Angew. Chem. Int. Edn* **44** 5997–6001
[21] Chen K H, Pu Y C, Chang K D, Liang Y F, Liu C M, Yeh J W, Shin H C and Hsu Y J 2012 Ag-nanoparticle-decorated SiO_2 nanospheres exhibiting remarkable plasmon-mediated photocatalytic properties *J. Phys. Chem.* C **116** 19039–45
[22] Yan J, Yang L P, Lin M F, Ma J, Lu X H and Lee P S 2013 Polydopamine spheres as active templates for convenient synthesis of various nanostructures *Small* **9** 596–603
[23] Lu L H and Eychmuller A 2008 Ordered macroporous bimetallic nanosctructures: design, characterization, and applications *Acc. Chem. Res.* **41** 244–53
[24] Yang S K, Cai W P, Kong L C and Lei Y 2010 Surface nanometer-scale patterning in realizing large-scale ordered arrays of metallic nanoshells with well-defined structures and controllable properties *Adv. Funct. Mater.* **20** 2527–33
[25] Dai Z F, Li Y, Duan G T, Jia L C and Cai W P 2012 Phase diagram, design of monolayer binary colloidal crystals, and their fabrication based on ethanol-assisted self-assembly at the air/water interface *ACS Nano* **6** 6706–16
[26] Plettl A, Enderle F, Saitner M, Manzke A, Pfahler C, Wiedemann S and Ziemann P 2009 Non-close-packed crystals from self-assembled polystyrene spheres by isotropic plasma etching: adding flexibility to colloid lithography *Adv. Funct. Mater.* **19** 3279–84
[27] Park H, Shin D, Kang G, Baek S, Kim K and Padilla W J 2011 Broadband optical antireflection enhancement by integrating antireflective nanoislands with silicon nanoconical-frustum arrays *Adv. Mater.* **23** 5796–800
[28] He H, Cai W P, Lin Y X and Dai Z F 2011 Silver porous nanotube built three-dimensional films with structural tunability based on the nanofiber template-plasma etching strategy *Langmuir* **27** 1551–5
[29] Liu G Q, Li Y, Duan G T, Wang J J, Liang C H and Cai W P 2012 Tunable surface plasmon resonance and strong SERS performances of Au opening-nanoshell ordered arrays *ACS Appl. Mater. Interfaces* **4** 1–5
[30] Ye X Z and Qi L M 2011 Two-dimensionally patterned nanostructures based on monolayer colloidal crystals: controllable fabrication, assembly, and applications *Nano Today* **6** 608–31
[31] Li Z Y, Tong W M, Stickle W F, Neiman D L and Williams R S 2007 Plasma-induced formation of Ag nanodots for ultra-high-enhancement surface-enhanced Raman scattering substrates *Langmuir* **23** 5135–8
[32] Ko H, Singamaneni S and Tsukruk V V 2008 Nanostructured surfaces and assemblies as SERS media *Small* **4** 1576–99
[33] Duan G T, Cai W P, Luo Y Y, Li Y and Lei Y 2006 Hierarchical surface rough ordered Au particle arrays and their surface enhanced Raman scattering *Appl. Phys. Lett.* **89** 181918
[34] Fang Y, Seong N H and Dlott D D 2008 Measurement of the distribution of site enhancements in surface-enhanced Raman scattering *Science* **321** 388–92
[35] He H, Cai W P, Lin Y X and Chen B S 2010 Au nanochain-built 3D netlike porous films based on laser ablation in water and electrophoretic deposition *Chem. Commun.* **46** 7223–5
[36] He H, Cai W P, Lin Y X and Chen B S 2010 Surface decoration of ZnO nanorod arrays by electrophoresis in the Au colloidal solution prepared by laser ablation in water *Langmuir* **26** 8925–32
[37] Zhang B H, Wang H S, Lu L H, Ai K K, Zhang G and Cheng X L 2008 Large-area silver-coated silicon nanowire arrays for molecular sensing using surface-enhanced Raman spectroscopy *Adv. Funct. Mater.* **18** 2348–55
[38] Wang Y Q, Yan B and Chen L X 2013 SERS tags: novel optical nanoprobes for bioanalysis *Chem. Rev.* **113** 1391–428
[39] Banholzer M J, Millstone J E, Qin L D and Mirkin C A 2008 Rationally designed nanostructures for surface-enhanced Raman spectroscopy *Chem. Soc. Rev.* **37** 885–97
[40] Mcnay G, Eustace D, Smith W E, Faulds K and Graham D 2011 Surface-enhanced Raman scattering (SERS) and surface-enhanced resonance Raman scattering (SERRS): a review of applications *Appl. Spectrosc.* **65** 825–37
[41] Sharma B, Frontiera R R, Henry A, Ringe E and Van Duyne R P 2012 SERS: materials, applications, and the future *Mater. Today* **15** 16–25